

PHYSICS

Surfactants and rotelles in active chiral fluids

Christian Scholz^{1*}, Anton Ldov¹, Thorsten Pöschel², Michael Engel², Hartmut Löwen¹

Surfactant molecules migrate to interfaces, reduce interfacial tension, and form micelles. All of these behaviors occur at or near equilibrium. Here, we describe active analogs of surfactants that operate far from equilibrium in active chiral fluids. Unlike molecular surfactants, the amphiphilic character of surfactants in active chiral fluids is a consequence of their activity. Our fluid of choice is a mixture of spinners that demixes into left-handed and right-handed chiral fluid domains. We realize spinners in experiment with three-dimensionally printed vibrots. Vibrot surfactants are chains of vibrots containing both types of handedness. Experiments demonstrate the affinity of double-stranded chains to interfaces, where they glide along and act as mixing agents. Simulations access larger systems in which single-stranded chains form spinning vesicles, termed rotelles. Rotelles are the chiral analogs of micelles. Rotelle formation is a ratchet mechanism catalyzed by the vorticity of the chiral fluid and only exist far from equilibrium.

INTRODUCTION

The structural and rheological properties of immiscible liquid mixtures (such as water and oil) can be tuned and controlled by adding surfactant molecules. Surfactants typically are amphiphilic; i.e., they have an asymmetric chemical structure with opposite preference for the two liquids. The surfactant is then driven to the liquid-liquid interface (1). For their abilities to emulsify immiscible liquids, to suspend dirt, and to protect colloids from coagulation, the application potential of surfactants is widespread in detergents, soaps, and cosmetic products. Notably, adding surfactants is an important route to designing new materials such as emulsions and self-assembled mesophases.

A second, complementary route for designing materials is based on actively driven degrees of freedom. Active matter is composed of particles that convert energy to create motion (2) and complex emergent behavior (3). An important class are self-propelled particles, which convert energy into translational motion. Such particles cluster as a consequence of their activity and phase separate into high-density and low-density domains (4, 5) and exhibit collective motion (6). Another class of active particles are spinners, which convert energy into rotational motion. We call the sense of rotation (clockwise or counterclockwise) the handedness of the spinner. A fluid of spinners with unique handedness is an example of a chiral fluid (7, 8), i.e., a fluid where the constituent particles are chiral. It has been found that a mixture of spinners with both types of handedness spontaneously demixes into two chiral fluids of opposite handedness (9–12). The reason for such demixing is the emergence of hydrodynamic (13) or mechanical (9) interactions resulting from activity.

The dynamic behavior of active chiral fluids is highly complex. Most notably, active chiral fluids exhibit active turbulence (14), aster-like vortices and rotating flocks (15–17), odd viscosity in the bulk (8), and enhanced surface flow near surfaces and interfaces (18–20). Chiral fluids have been experimentally realized at different scales (7, 12, 21–26). A particularly intriguing example at the macroscale uses miniature robots called bristlebots or vibrobots that convert

vibration into forward motion by hopping on tilted elastic legs (27, 28). By changing the legs' orientations, bristlebots can be manufactured to convert vibration into both translational and rotational motion. Bristlebots that rotate are called vibrots (29–32). Vibrots must have a chiral leg configuration to rotate and can be designed for both senses of rotation (12).

The potential of active matter has been extended by self-assembled chains of active particles or active filaments. For instance, chains of self-propelled swimmers were realized using magnetic microparticles (33), and Janus colloids can be chained with induced polar charge distribution (34). Organisms, such as *Tubifex tubifex* worms, are biological examples of active filaments (35). Active polymers show tunable, activity-induced dynamics (36–39). Closed chains of vibrots have been studied computationally as a means to compartmentalize vibrot dynamics similar to biological cells (40).

Here, we report complex self-organization phenomena in active chiral fluids made from vibrots induced by the addition of vibrot chains. Because active chiral fluids are most different from conventional (non-chiral) fluids near interfaces, we develop and investigate nonequilibrium analogs of molecular surfactants. To design surfactants in chiral vibrot fluids, we implement simultaneous affinity to both types of handedness. Such an emergent amphiphilicity attracts these vibrot surfactants to interfaces between domains of left-handed and right-handed vibrots. We realize vibrot surfactants as chains containing both types of handedness.

Our experiments on a vibrating plate and Langevin dynamics simulations demonstrate that suitably designed vibrot chains mimic several behaviors of amphiphilic molecules in alternative ways. Depending on the chain geometry, vibrot surfactants can show different phenomena: (i) Double-stranded vibrot chains with each strand of opposite handedness act as mixing agents. In contrast to molecular surfactants, vibrot surfactants remain in directed translational motion and glide along interfaces. This means that vibrot surfactants cannot form micelles. (ii) Single-stranded vibrot chains with two blocks, one of each handedness (reminiscent of block copolymers), can close in around vibrots and form spinning vesicles. We call such a spinning vesicle a rotelle. The term “rotelle” is derived from Latin for “little wheel” and a portmanteau of the words rotation and micelle. The transition from chains to rotelles is caused by irreversible jamming of vibrots at the rotelle surface, a process reminiscent of a ratchet mechanism. We start with simple vibrot chain

Copyright © 2021 The Authors, some rights reserved; exclusive licensee American Association for the Advancement of Science. No claim to original U.S. Government Works. Distributed under a Creative Commons Attribution NonCommercial License 4.0 (CC BY-NC).

¹Institut für Theoretische Physik II: Weiche Materie, Heinrich-Heine-Universität Düsseldorf, 40225 Düsseldorf, Germany. ²Institute for Multiscale Simulation Friedrich-Alexander-Universität Erlangen-Nürnberg, 91058 Erlangen, Germany.

*Corresponding author. Email: christian.scholz@hhu.de

geometries and gradually advance towards more complex geometries revealing even more complex self-organization phenomena.

RESULTS

Dimers suppress vibrot demixing

One of the most intriguing phenomena in systems of vibrots is the demixing of left-handed and right-handed vibrots. Demixing is an emergent phenomenon with origin in the activity of the vibrots (9–12): Two colliding vibrots can block each other's rotation and get stuck. It is found that the contact time of equal-handed vibrots is substantially longer than the contact time between two oppositely handed vibrots (9). The result is an emergent attraction between equal-handed vibrots. Clearly, demixing must be affected by rigid connectors between vibrots. We test this hypothesis in experiment and simulation.

We introduce dimers (two connected vibrots of opposite handedness; Fig. 1A) into a mixed vibrot fluid and analyze the tendency of vibrots to demix as a function of the number of dimers. We start from a disordered system of vibrot monomers and run the system until it approaches a steady state in the demixed state. Then, we add some connectors and equilibrate the system again. To reach a steady state, only a few connectors are added at each step and we let the system run until individual monomers and dimers moved across the whole system several times (fig. S1). This addition of connectors is repeated until all monomers are converted into dimers. Three snapshots of the system are shown in Fig. 1B: the demixed state without dimers, an intermediate fraction of dimers, and the pure dimer configuration. The dynamics of the system is shown in movies S1 to S3.

Whereas the monomer system approaches complete demixing, adding dimers continuously decreases the chiral fluid domain size. We quantify the demixing tendency of vibrots by counting the average number of equal neighbors, i.e., neighbors with identical sense of rotation, $\langle N_{eq} \rangle$, and the number of chiral fluid domains N_d as a function of the fraction of dimers in the system (Fig. 1, C and D, and fig S1). Vibrots are identified as neighbors if they are connected by an edge in the Delaunay triangulation of the vibrot centers (41). As a reference, the system is compared to a hypothetical random configuration that is obtained by randomly shuffling the handedness of all vibrots (gray line in the figure). As expected, the number of equal neighbors $\langle N_{eq} \rangle$ decreases, and the number of chiral fluid domains N_d increases with dimer fraction. At dimer fraction around 0.5, $\langle N_{eq} \rangle$ crosses the random reference and N_d reaches a maximum. At this dimer fraction, the system resembles a random mixture most closely. For even higher dimer fractions, both $\langle N_{eq} \rangle$ and N_d decrease, likely because vibrots of opposite handedness are forced to remain in contact by the connectors. However, above dimer fractions of 0.5, the spatial distribution of particles remains similar to the random configuration and no further structure formation or nematic order is observed. Consequently, we refer to this state as the mixed phase. These findings demonstrate that adding dimers is a strategy to control vibrot demixing.

Double-stranded chains remain at the interface

We investigate more complex chain geometries in the form of double-stranded vibrot chains. In these chains, each strand has opposite handedness. Double-stranded chains migrate to interfaces where the left-handed and right-handed strands can be in contact with

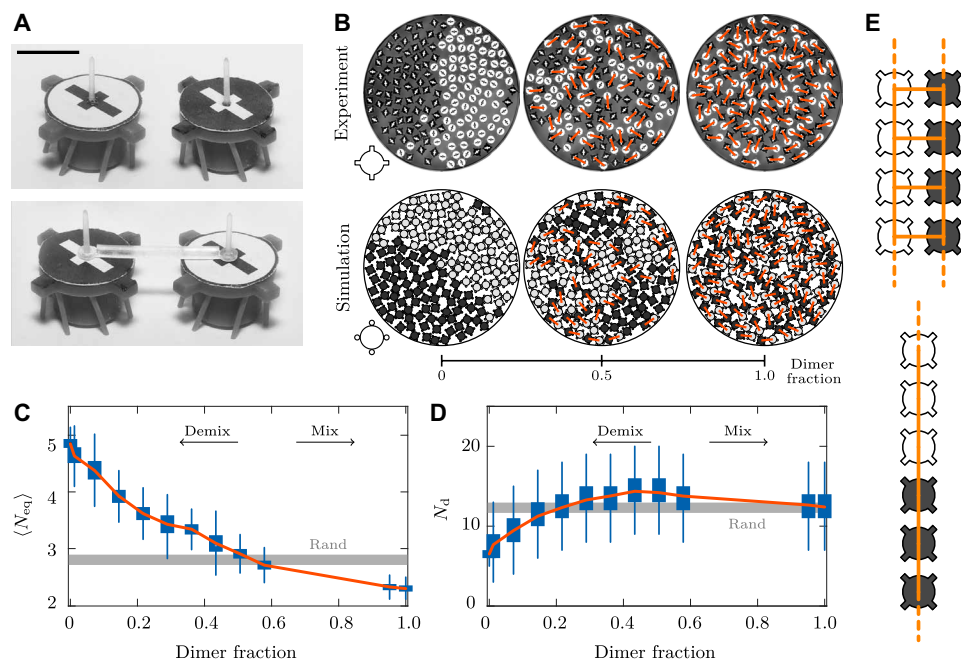


Fig. 1. Vibrot dimers suppress demixing of vibrot fluids. (A) Left-handed (black with white cross) and right-handed (white with black cross) vibrots manufactured by 3D printing (top). Scale bar, 10 mm. Vibrots can be connected by rigid bars that do not affect rotations (bottom). (B) Snapshots of equilibrated systems with increasing fractions of dimers. Connectors are highlighted by orange lines. Insets illustrate the particle geometry in experiments and simulations respectively. (C) Average number of equal neighbors per vibrot $\langle N_{eq} \rangle$ and (D) number of chiral fluid domains N_d . The gray line corresponds to the hypothetical random state in which the handedness of all vibrots has been shuffled. Boxes indicate the 25th and 75th percentiles (p_{25} and p_{75}). Whiskers show the range of observations from maximum to minimum. Points outside of $[p_{25} - 1.5(p_{75} - p_{25}), p_{75} + 1.5(p_{75} - p_{25})]$ are discarded as outliers. (E) Illustration of double-stranded and single-stranded chain configurations.

left-handed and right-handed vibrot fluids, respectively. We first test double-stranded chains in small systems in experiments and then advance to larger systems in simulations.

We add $3N - 2$ connectors to create a vibrot chain of geometry $2 \times N$ (Figs. 1E and 2A). The omission of diagonal connectors allows the chains to remain flexible and bend at right angles. Experiments start with a single long double-stranded chain of length $N = 14$ located across the center of the vibrating plate. Vibrot monomers are distributed in the remaining space in a mixed state (Fig. 2B). After turning on vibration, vibrots migrate along the chain, and the system demixes rapidly (Fig. 2B and movie S4). The evolution of the center of mass distances between the two vibrot fluids and the chain quantifies the demixing progress (Fig. 2C).

We observe in the demixed state that the two strands of the chain face domains with opposite handedness. We explain this counterintuitive phenomenon as follows: Vibrots in the two chiral fluids near the chain and near the confinement boundary move collectively in a circular fashion. Similar enhanced surface flow is found already in the absence of the chain (movie S1) (12, 18). Because the chain is kept stationary by our experimental setup (a consequence of the circular boundary), it cannot be dragged along with the surface flow. We noticed that the stationary chain inhibits surface flow if strands face chiral fluids of equal handedness but supports surface flow in the opposite orientation. We observe the latter orientation in our experiment, which indicates that it is preferable. The contact of the left-handed side of the chain to a right-handed chiral fluid (and vice versa) is in stark contrast to the common behavior of surfactants. For this reason, we call this behavior the anti-surfactant behavior. We note that the anti-surfactant behavior of vibrot chains has also been found in simulations of active colloidal cells (40) and is now reproduced in our experiments.

To demonstrate this analogy, we investigate two situations: first, a (monodisperse) boundary with 38 right-handed vibrots, and second, a Janus (two chiral halves) boundary with 19 left-handed vibrots and 19 right-handed vibrots. The remaining vibrots are confined to the inside.

We start the experiment in a mixed configuration (Fig. 3A). Vibrots with handedness equal to the handedness of the boundary migrate towards the boundary. After about 500 s, right-handed

vibrots are found on average at a notably larger distance from the center than left-handed vibrots, in perfect agreement with simulations (Fig. 3B). This core-shell configuration then persists for the rest of the measurement. Because of the enhanced surface flow, the boundary rotates once the core-shell configuration has formed. As a consequence, the boundary vibrots and the vibrots in the interior can flow side by side in a quasi-laminar fashion. These results demonstrate an emergent attraction between boundary vibrots and vibrots in the interior with the same handedness (Fig. 3C). We conclude that a boundary that follows the flow of a chiral fluid causes common surfactant behavior.

For the Janus boundary, the situation is completely different. The Janus boundary cannot rotate because such rotation would break the symmetry of the setup. The boundary disturbs the chiral fluid and affects how it interacts with the boundary. Experiment (Fig. 3D) and simulation (Fig. 3E) now form two chiral fluid domains in the shape of half-disks instead of a core-shell configuration. As in previous simulation work (40), the location of the chiral fluid interface fluctuates noticeably and individual vibrots tend to break off from one side and migrate along the boundary until they emerge back from the other side. These results demonstrate an emergent repulsion between boundary vibrots and vibrots in the interior with the same handedness (Fig. 3F).

Our experiments demonstrate that double-stranded chains have a strong affinity to the interface, owing to the anti-surfactant interaction with the surface flows. However, because of practical limitations and the need for a boundary, we can only study a few short double-stranded chains in this way (fig. S2). Hence, the strong presence of boundary effects in the experiment, in particular the edge currents (18), raise the question, how active surfactants behave in a true bulk system. The next section will eliminate the experimental restrictions and grant access to much larger system sizes in simulations.

Effect of double-stranded chains on demixing

We resort to simulations of larger systems with periodic boundary conditions to study self-organization phenomena in the absence of the circular boundary that limits our experiments. Initial vibrot configurations are created in two steps: First, double-stranded chains (geometry $2 \times N$ with chain length N) are placed in the simulation

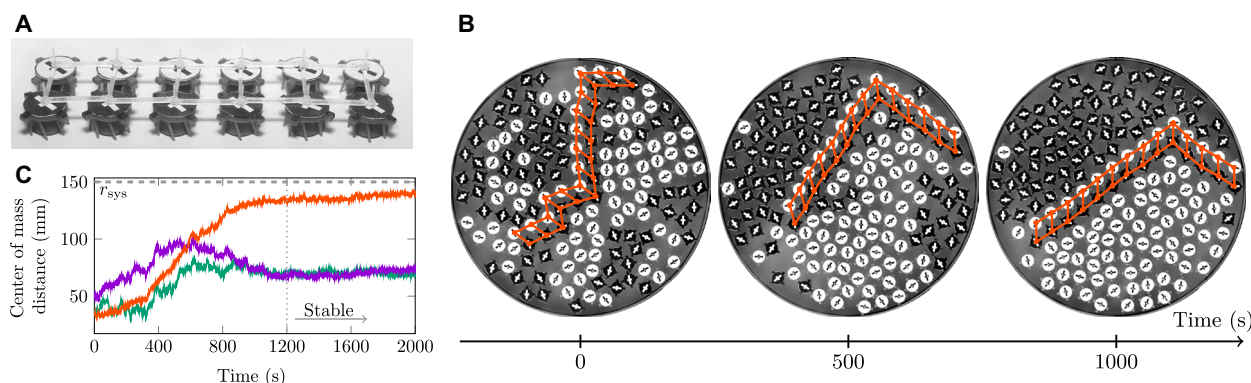


Fig. 2. Double-stranded vibrot chains have an affinity for chiral vibrot fluid interfaces. (A) Double-stranded vibrot chain of geometry 2×6 . Strands are made from vibrots of opposite handedness. Vibrots are connected to their nearest neighbors in a square lattice to keep the chain semi-flexible. (B) Experimental snapshots with a 2×14 chain at three observation times. Vibrots are positioned initially in the mixed phase and then demixed. Orange lines are connectors. (C) Evolution of the distance between the centers of mass of the left-handed and right-handed fraction of vibrots (orange curve). Distance of each fraction from the chain's center of mass (purple and green). All distances approach a constant. The distance between the fraction remains slightly below the confinement radius $r_{sys} = 150$ mm.

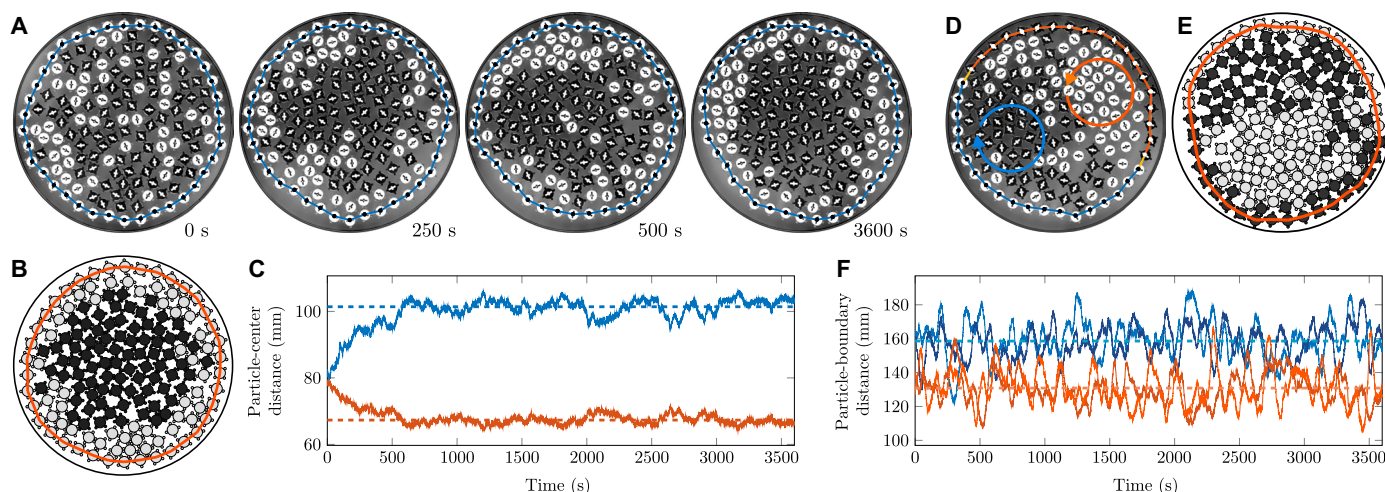


Fig. 3. Demixing of a vibrot fluid in the presence of an active boundary. (A) Snapshots of the experiment at 0, 250, 500, and 3600 s. Left-handed vibrots are black with white crosses. Right-handed vibrots are white with black crosses. (B) Snapshot of the simulation after steady state has been reached. (C) Average distance of vibrots from the center of mass of the entire system for left-handed vibrots (orange) and right-handed vibrots (blue). Right-handed vibrots collect preferably at the boundary that consists of vibrots with the same handedness. (D) Snapshot of the experiment after steady state has been reached. Vibrots are found predominantly near boundary regions made from vibrots of opposite handedness. This is explained by the commensurability of the collective flow of the demixed domains (blue and orange circles) to the rotation direction of vibrots at the boundary. (E) Snapshot of the simulation after steady state has been reached. (F) Average distances of vibrots in the interior from vibrots in the boundary. Blue and red curves correspond to the distances for vibrots of equal and opposite handedness, respectively. Vibrots of opposite handedness show, on average (dashed lines), a smaller distance than vibrots of equal handedness.

box. Second, the remaining space is filled with monomers of randomly chosen handedness up to packing fraction 50% keeping a mixing ratio of exactly 1:1. The total system contains 2348 vibrot monomers, among them 1174 vibrots of each handedness. The chain concentration, P , is defined as the number of vibrots in all chains divided by the total number of vibrots in the system. This setup allows us to analyze vibrot demixing and chain dynamics as a function of the two remaining parameters chain length, N , and chain concentration, P .

We start with chains of medium length, $N = 6$. At concentration $P = 6\%$, the number of chains is too low to affect vibrot demixing substantially. Demixing occurs via spinodal decomposition (9), and we simulate five times longer than necessary to reach steady state. After demixing is complete, only a few chains remain fully immersed in a chiral fluid. Most of the chains are found at or near interfaces (Fig. 4A and movie S5). This observation demonstrates the affinity of double-stranded chains to interfaces. Chains have each strand in contact with a chiral fluid of the same handedness as expected from common surfactant behavior. The anti-surfactant behavior observed in the experiment of Fig. 2 disappeared because chains can now translate in the absence of a boundary. The presence of translation motion shows that double-stranded chains act as microswimmers in active chiral fluids.

We observe two clearly distinct modes of chain motion (Fig. 4A): (i) Chains inside active chiral fluids strive to minimize contact of oppositely handed vibrots. As a result, they bend and move in circles; i.e., they behave like circle swimmers (42). (ii) In contrast, chains at interfaces remain straight and glide along the interface (43) with maximum velocity; i.e., they perform superdiffusive motion. Chains can even surf on interfacial waves and dive back into the chiral fluids (movie S5). Once demixing is complete, circular swimming and superdiffusive motion can persist over long time intervals. Chains switch back and forth between both modes of motion

as apparent by straight horizontal and vertical segments in the translation versus rotation trajectory plot (Fig. 4A).

Straight segments in the trajectory plot disappear as we increase the concentration of double-stranded chains, first to 18% and then to 30% (Fig. 4, B and C). The disappearance is caused by the suppression of vibrot demixing. Chains that swim along and through the interface drag some monomers along and keep the system mixed (movie S6). This means that double-stranded chains destabilize interfaces not by lowering interfacial tension, as is the case for molecular surfactants, but by acting as mixing agents for vibrot fluids. Because of their destabilizing effect on interfaces, we term our double-stranded vibrot chains as vibrot surfactants.

We analyze the destabilizing effect of vibrot surfactants systematically by scanning the two-dimensional (2D) parameter space spanned by the chain length, N , and the chain concentration, P , in the ranges $1 \leq N \leq 12$ and $3\% \leq P \leq 36\%$. The parameter space map in Fig. 4D and fig. S3 demonstrates that double-stranded chains suppress demixing once the concentration of vibrot surfactants is sufficiently high, about 15 to 25%, depending on the chain length, N .

Rotelle formation

Molecular surfactants are versatile building blocks for higher-order self-assembled mesophases. Examples are spherical micelles, lipid bilayers, and gyroid networks. Because vibrot surfactants have a strong destabilizing effect on active chiral fluids, they do not seem to form any higher-order structures. The origin of the destabilization is the swimming motion of vibrot surfactants. Therefore, chains of other geometry that do not swim must be implemented to observe previously unidentified self-organization phenomena.

Single-stranded vibrot chains that contain two blocks of vibrots of identical handedness, one block for each (Fig. 1E), are one such suitable geometry. It is reminiscent of block copolymers at the

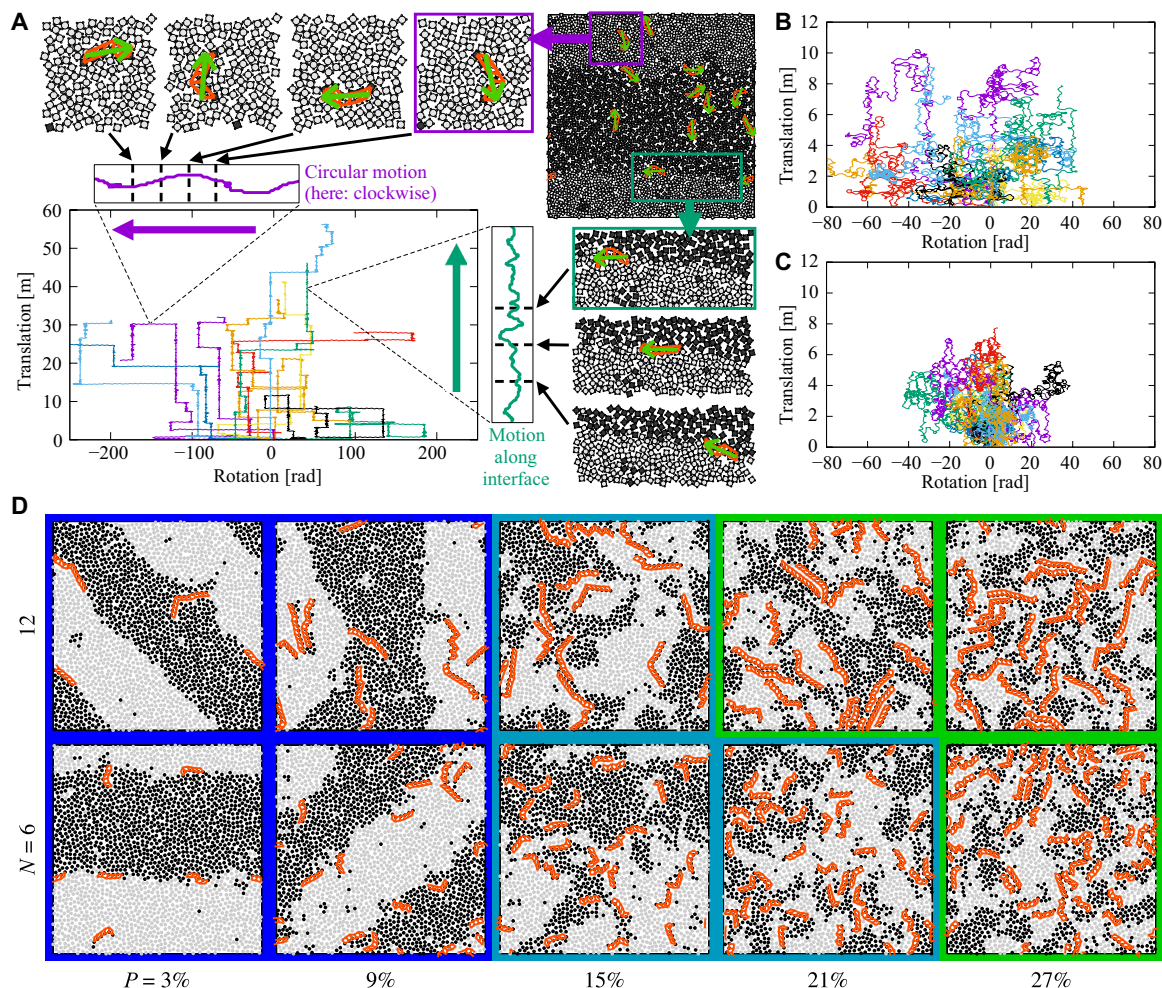


Fig. 4. Double-stranded vibrot chains act as mixing agents for vibrot fluids. (A) Analysis of chain motion in a simulation with complete demixing (chain length $N=6$, chain concentrations $P=6\%$). We identify the center of mass and the orientation of each chain (green arrow) and measure the total move distance from the start position (labeled as translation) and the total orientation change (labeled as rotation). Two modes of chain motion can be clearly distinguished in the translation versus rotation trajectory plot (bottom left): circular motion inside chiral fluids (top left; horizontal segments in trajectory plot) and superdiffusive motion along interfaces (bottom right; vertical segments). (B) The trajectory plot for a system with partial demixing (chain concentrations, 18%) has shorter straight segments indicating smaller chiral fluid domain sizes. Note the smaller axis ranges. (C) The trajectory plot for a system that remains mixed (chain concentrations, 30%) is evidence for free diffusion. Each trajectory plot contains the trajectories of 12 randomly chosen chains sampled over a time of 10^4 s. (D) Final simulation snapshots reveal complete demixing (dark blue frames), partial demixing (light blue frames), and no demixing (green frames) as a function of chain length N and chain concentration P . Vibrots are shown as disks for faster rendering.

molecular scale. Our computer simulations reveal that single-stranded block chains do not migrate to interfaces. In principle, each block has an affinity to the corresponding equal-handed chiral fluid. However, sufficiently long chain blocks extend far from the interface into the fluids. As a result, single-stranded block chains inhibit surface flow. This destabilizes interfaces and drives the chains away.

The potential of single-stranded vibrot block chains for self-organization lies in the nature of active chiral fluids: Chiral fluids have odd viscosity (8) and exhibit active turbulence (14). We observe a high propensity of single-stranded block chains to rotate and act as sources of vorticity. This behavior is most prominent if the chains are embedded in a chiral fluid (movies S7 and S8). These simulations demonstrate a previously unreported self-organization phenomenon, the formation of rotelles. The basic mechanism is illustrated in Fig. 5A. Single-stranded vibrot block chains rotating in the

chiral fluid can spontaneously surround vibrot monomers. Once the chain closes far enough, the rotations of the vibrots pull the chain together further, firmly encapsulating their interior. The resulting vesicle-like aggregates remain stable after formation even if the vibrots forming the surrounding fluid are completely removed. This demonstrates that vesicle formation requires overcoming a kinetic barrier and is irreversible; in other words, the process is reminiscent of nonequilibrium ratchet mechanisms (44). Vesicles in a vibrot fluid spin as a single block because they feel the forces of adjacent monomers, motivating the rotelle terminology.

Rotelles occur in different sizes and forms (Fig. 5B). In the most compact rotelles, only the chain itself has curled up (Fig. 5C). Compact rotelles, though rather fragile, occur in particular for relatively short chains. More rare observations are onion-like double-chain enclosures. Rotelles can even have a Janus character, in which case each block curls up by itself.

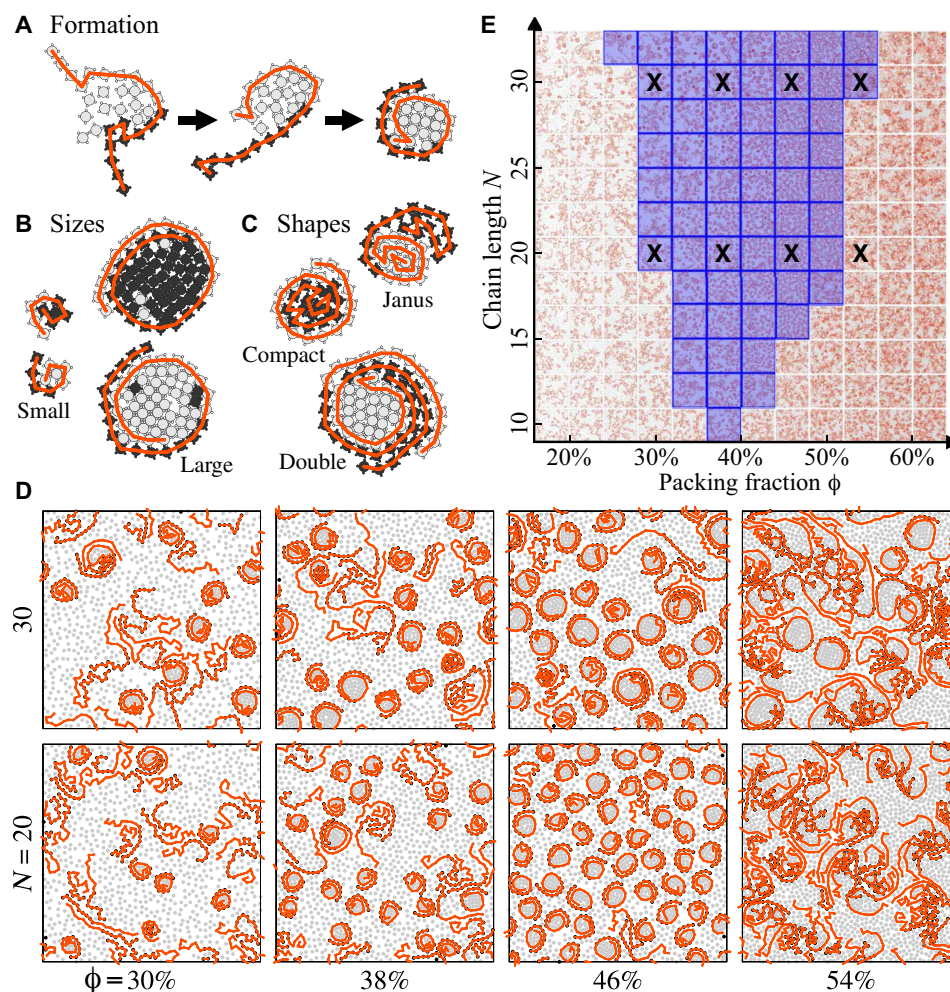


Fig. 5. Rotelle formation in single-stranded vibrot block chains. (A) Single-stranded vibrot chains made from two blocks of opposite handedness can close around vibrot monomers and form a stable rotelle. (B) Rotelles appear in different sizes and can turn either of their blocks to the outside. The vibrots caught in the inside predominantly are of the handedness of the inside block. (C) More exotic but also much rarer rotelles observed in simulation. (D) Snapshots of a simulation with block-copolymer chains of varying chain length, N , and packing fraction, ϕ . We observe a concentrated rotelle solution at packing fraction $\phi = 46\%$. The chain concentration is kept constant at $P = 50\%$. Vibrots are shown as disks for faster rendering. (E) Parameter space map. Rotelles form best at intermediate packing fractions (blue). "X" marks the snapshots shown in (D). A vector graphic is found in fig. S4.

Rotelle formation occurs only at sufficiently high packing fraction (density) and is catalyzed by vorticity. At low and high packing fraction, vorticity is too low and rotelles cannot form. The parameter space map (Fig. 5, D and E, and fig. S4) demonstrates that rotelles form robustly for chains of length $N > 10$ and in a packing fraction range that widens with N . The first rotelles in Fig. 5D form quickly and reproducibly. Their presence lowers the density of the surrounding chiral fluid. This means that the formation of additional rotelles becomes more and more difficult over time. Nevertheless, for long enough chains and at high density near 50% packing fraction, most of the vibrots are eventually captured in rotelles (fig. S4). Rotelles also form in mixed vibrot fluid (fig. S5). The process then takes longer and the number of rotelles is typically lower.

DISCUSSION

Our observation could be exploited for self-assembly in active mesoparticles down to the colloidal length scale. Sophisticated control

mechanisms are required to make such particles perform tasks autonomously, for example, those investigated in this work. Rotelles could encapsulate cargo particles and release them at a desired location by reducing the activity and let them disentangle. However, this will require a 3D generalization of the mechanism. The swimming mechanism of the surfactants dynamically changes the structure of a chiral fluid by tuning the size of demixed domains, with potential applications in the synthesis of intelligent materials.

Downsizing spinner chains is a challenge but might be achieved by appropriate new techniques. Rotating microparticles have been manufactured in various ways (16, 24, 26, 45, 46). Adding connectors between particles is possible in principle (47–49). However, connectors might not even be necessary. For example, the effect of spinner rotation in a chain can be reproduced by the movement of suitably designed flagella attached to the surface of a rod. It remains an open question, whether the dynamics of the system are stable against the hydrodynamic and electrostatic forces that are typically present for colloidal particles.

In conclusion, we demonstrated a previously unknown strategy to engineer active matter taking inspiration from the equilibrium behavior of molecular surfactants. This is analogous to generating new materials at the atomic scale by using polymers and other (macro) molecules. The addition of vibrot chains modifies the dynamics of vibrot fluids and create unexpected self-organization phenomena. Activity and choice of chain geometry are responsible for the amphiphilic character of the chains and can be controlled externally (activity) or by deliberate choice (chain geometry). In contrast to molecular surfactants, vibrot surfactants must be driven by a source of energy to perform their function. They demonstrate a striking example of complex structure formation in granular systems that even mimic polymers, but on a much larger length scale and far away from equilibrium. Vibrot surfactants do not lower interfacial tension but act as mixing agents. Vibrot block chains self-organize into rotelles irreversibly by a ratchet mechanism. Rotelles take the place of micelles, which do not form in our chiral fluid. Notably, rotelles can themselves be considered self-spinning particles of a higher degree of complexity and could again be used as building blocks for larger and more complex structures. The granular experiments and simulations in this work provide first insights into the phenomenology that can be achieved with suitably designed building blocks in active chiral fluids. Future work can combine translation and spinning and extend this work to three dimensions, by combining chiral shapes and active motion, to realize even richer behavior.

METHODS

Experimental setup

Experiments are performed with vibrots excited to rotate by vertical vibrations of a horizontal plate. Our vibrot design (Fig. 1A) is optimized for manufacturing via 3D printing (12, 30, 31). The body of the vibrot consists of two stacked cylinders (top $d = 15$ mm, $h = 2$ mm; bottom $d = 11$ mm, $h = 6$ mm). Seven legs (length, 8.5 mm; diameter, 1 mm) are attached at regular angles to the top cylinder, tilted in tangential direction by 18° . The tilt direction determines the sense of rotation. We denote vibrots as left-handed if they spin clockwise and right-handed if they spin counterclockwise. To introduce mechanical interactions between vibrots, four equidistant rectangle-shaped cantilevers (length, 3 mm) are attached to the top cylinder. Vibrots are printed using a stereolithographic 3D printer (Formlabs Form 2 with Formlabs Grey V3, FLGPR03 resin). A single vibrot weighs approximately 1 g. Vibrations are provided by an electromechanical shaker (Tira TV 51140) at a frequency of 80 Hz and an amplitude of 2.1(1)g (measured using a LIS3DH accelerometer), similar to the values used in (12). Vibrots are enclosed on the vibrated plate by a circular boundary of diameter 30 cm. All experiments are performed with a system of 83 left-handed and 83 right-handed vibrots, which corresponds to an area fraction of about 50%. At this packing fraction, demixing is observed robustly.

To create chains, each vibrot has a small pin in the center on top, which can hold one or several rigid connectors (bars with a ring at each end; Fig. 1A). Connectors do not slow down rotation and have a hole-to-hole distance of 22 mm. Connectors are 3D-printed using clear resin to make them as transparent as possible. To detect connectors robustly via computational image processing, we record the system over an extended period at frame rates of 10 to 30 Hz using a digital camera (Allied Vision Mako-U130B) and identify trajectories that have a constant distance throughout the measurement. 3D

model files of vibrots and connectors are included as Supplementary Materials.

Simulation setup

Vibrots in simulations consist of five disks with total area of a simulated vibrot equal to the horizontal cross section of a 3D-printed vibrot ($d_1 = 15$ mm, $d_{2-5} = 3.4$ mm, see the insets of Fig. 1B). Past simulations reproduced the experimental observation of demixing in vibrots quantitatively (9, 12). As in these works, we model vibrot dynamics by a system of coupled Langevin dynamics equations

$$M \frac{d\mathbf{v}_i}{dt} = \mathbf{F}_i + \gamma^T (\sqrt{2D^T} \boldsymbol{\eta}_i(t) - \mathbf{v}_i) \quad (1)$$

$$I \frac{d\boldsymbol{\omega}_i}{dt} = \boldsymbol{\tau}_i + \gamma^R (\sqrt{2D^R} \boldsymbol{\zeta}_i(t) - \boldsymbol{\omega}_i) + \boldsymbol{\tau}_i^D \quad (2)$$

for its degrees of freedom, x, y, ϕ , driven by an external torque $\boldsymbol{\tau}_i^D = \pm \boldsymbol{\tau}$. M and I are mass and moment of inertia, $\mathbf{v}_i = (\partial x_i / \partial t, \partial y_i / \partial t)$ and $\boldsymbol{\omega}_i = \partial \phi / \partial t$ are the translational and rotational velocities, \mathbf{F}_i and $\boldsymbol{\tau}_i$ are the interaction forces and torques, and γ^T, γ^R are translational and rotational damping coefficients. Each particle is also subject to a random uncorrelated force $\boldsymbol{\eta}_i$ and torque $\boldsymbol{\zeta}_i$ to model the erratic motion of individual particles in the absence of collisions. The magnitude is quantified by the translational diffusion constant D^T and rotational diffusion constant D^R .

Vibrots have the same geometry, mass, and moment of inertia as in the experiment and interact via an elastic Hertzian contact force. Chains are connected via harmonic springs with spring constant $k = 100$ N/m to mimic the rigid connectors used in the experiment. Force parameters are chosen as in (12) except for the Young's modulus $Y = 10$ kPa. At this value, vibrots behave as quasi-hard particles in good agreement with experiments.

SUPPLEMENTARY MATERIALS

Supplementary material for this article is available at <http://advances.sciencemag.org/cgi/content/full/7/16/eabf8998/DC1>

REFERENCES AND NOTES

1. J. N. Israelachvili, *Intermolecular and Surface Forces* (Elsevier, 2011).
2. C. Bechinger, R. Di Leonardo, H. Löwen, C. Reichhardt, G. Volpe, G. Volpe, Active particles in complex and crowded environments. *Rev. Mod. Phys.* **88**, 045006 (2016).
3. A. Zöttl, H. Stark, Emergent behavior in active colloids. *J. Phys. Condens. Matter* **28**, 253001 (2016).
4. J. Palacci, S. Sacanna, A. P. Steinberg, D. J. Pine, P. M. Chaikin, Living crystals of light-activated colloidal surfers. *Science* **339**, 936–940 (2013).
5. I. Buttinoni, J. Bialké, F. Kümmel, H. Löwen, C. Bechinger, T. Speck, Dynamical clustering and phase separation in suspensions of self-propelled colloidal particles. *Phys. Rev. Lett.* **110**, 238301 (2013).
6. J. Deseigne, O. Dauchot, H. Chaté, Collective motion of vibrated polar disks. *Phys. Rev. Lett.* **105**, 098001 (2010).
7. S. Fürthauer, M. Stempel, S. W. Grill, F. Jülicher, Active chiral fluids. *Eur. Phys. J. E* **35**, 89 (2012).
8. D. Banerjee, A. Souslov, A. G. Abanov, V. Vitelli, Odd viscosity in chiral active fluids. *Nat. Commun.* **8**, 1573 (2017).
9. N. H. P. Nguyen, D. Klotsa, M. Engel, S. C. Glotzer, Emergent collective phenomena in a mixture of hard shapes through active rotation. *Phys. Rev. Lett.* **112**, 075701 (2014).
10. K. Yeo, E. Lushi, P. M. Vlahovska, Collective dynamics in a binary mixture of hydrodynamically coupled microrotors. *Phys. Rev. Lett.* **114**, 188301 (2015).
11. S. Sabrina, M. Spellings, S. C. Glotzer, K. J. M. Bishop, Coarsening dynamics of binary liquids with active rotation. *Soft Matter* **11**, 8409–8416 (2015).
12. C. Scholz, M. Engel, T. Pöschel, Rotating robots move collectively and self-organize. *Nat. Commun.* **9**, 931 (2018).
13. Y. Fily, A. Baskaran, M. C. Marchetti, Cooperative self-propulsion of active and passive rotors. *Soft Matter* **8**, 3002 (2012).

14. G. Kokot, S. Das, R. G. Winkler, G. Gompper, I. S. Aranson, A. Snezhko, Active turbulence in a gas of self-assembled spinners. *Proc. Natl. Acad. Sci. U.S.A.* **114**, 12870–12875 (2017).
15. D. Levis, I. Pagonabarraga, B. Liebchen, Activity induced synchronization: Mutual flocking and chiral self-sorting. *Phys. Rev. Res.* **1**, 023026 (2019).
16. B. Zhang, A. Sokolov, A. Snezhko, Reconfigurable emergent patterns in active chiral fluids. *Nat. Commun.* **11**, 4401 (2020).
17. Z.-F. Huang, A. M. Menzel, H. Löwen, Dynamical crystallites of active chiral particles. *Phys. Rev. Lett.* **125**, 218002 (2020).
18. B. C. van Zuiden, J. Paulose, W. T. M. Irvine, D. Bartolo, V. Vitelli, Spatiotemporal order and emergent edge currents in active spinner materials. *Proc. Natl. Acad. Sci. U.S.A.* **113**, 12919–12924 (2016).
19. V. Soni, E. S. Billign, S. Magkiriadou, S. Sacanna, D. Bartolo, M. J. Shelley, W. T. M. Irvine, The odd free surface flows of a colloidal chiral fluid. *Nat. Phys.* **15**, 1188–1194 (2019).
20. C. Reichhardt, C. J. O. Reichhardt, Reversibility, pattern formation, and edge transport in active chiral and passive disk mixtures. *J. Chem. Phys.* **150**, 064905 (2019).
21. J.-C. Tsai, F. Ye, J. Rodriguez, J. P. Gollub, T. C. Lubensky, A chiral granular gas. *Phys. Rev. Lett.* **94**, 214301 (2005).
22. K. Drescher, K. C. Leptos, I. Tuval, T. Ishikawa, T. J. Pedley, R. E. Goldstein, Dancing volvox: Hydrodynamic bound states of swimming algae. *Phys. Rev. Lett.* **102**, 168101 (2009).
23. A. P. Petroff, X.-L. Wu, A. Libchaber, Fast-moving bacteria self-organize into active two-dimensional crystals of rotating cells. *Phys. Rev. Lett.* **114**, 158102 (2015).
24. M. Driscoll, B. Delmotte, M. Youssef, S. Sacanna, A. Donev, P. Chaikin, Unstable fronts and motile structures formed by microrollers. *Nat. Phys.* **13**, 375–379 (2017).
25. G. Kokot, A. Snezhko, Manipulation of emergent vortices in swarms of magnetic rollers. *Nat. Commun.* **9**, 2344 (2018).
26. K. Han, G. Kokot, S. Das, R. G. Winkler, G. Gompper, A. Snezhko, Reconfigurable structure and tunable transport in synchronized active spinner materials. *Sci. Adv.* **6**, eabz8535 (2020).
27. L. Giomi, N. Hawley-Weld, L. Mahadevan, Swarming, swirling and stasis in sequestered bristle-bots. *Proc. Roy. Soc. Lond. Ser. A* **469**, 20120637 (2013).
28. G. A. Patterson, P. I. Fierens, F. Sangiuliano Jimka, P. G. König, A. Garcimartin, I. Zuriguel, L. A. Pugnaloni, D. R. Parisi, Clogging transition of vibration-driven vehicles passing through constrictions. *Phys. Rev. Lett.* **119**, 248301 (2017).
29. E. Altshuler, J. M. Pastor, A. Garcimartin, I. Zuriguel, D. Maza, Vibrot, a simple device for the conversion of vibration into rotation mediated by friction: Preliminary evaluation. *PLOS ONE* **8**, e67838 (2013).
30. C. Scholz, S. D'Silva, T. Pöschel, Ratcheting and tumbling motion of vibrots. *New J. Phys.* **18**, 123001 (2016).
31. C. Scholz, T. Pöschel, Velocity distribution of a homogeneously driven two-dimensional granular gas. *Phys. Rev. Lett.* **118**, 198003 (2017).
32. M. Broseghini, C. Ceccolini, C. Della Volpe, S. Siboni, The Notched Stick, an ancient vibrot example. *PLOS ONE* **14**, e0218666 (2019).
33. A. Snezhko, I. S. Aranson, Magnetic manipulation of self-assembled colloidal asters. *Nat. Mater.* **10**, 698–703 (2011).
34. D. Nishiguchi, J. Iwasawa, H.-R. Jiang, M. Sano, Flagellar dynamics of chains of active Janus particles fueled by an AC electric field. *New J. Phys.* **20**, 015002 (2018).
35. A. Deblais, A. C. Maggs, D. Bonn, S. Woutersen, Phase separation by entanglement of active polymerlike worms. *Phys. Rev. Lett.* **124**, 208006 (2020).
36. A. Kaiser, S. Babel, B. ten Hagen, C. von Ferber, H. Löwen, How does a flexible chain of active particles swell? *J. Chem. Phys.* **142**, 124905 (2015).
37. T. Eisenstecken, G. Gompper, R. G. Winkler, Conformational properties of active semiflexible polymers. *Polymers* **8**, 304 (2016).
38. R. G. Winkler, J. Elgeti, G. Gompper, Active polymers—Emergent conformational and dynamical properties: A brief review. *J. Physical Soc. Japan* **86**, 101014 (2017).
39. M. Agrawal, S. C. Glotzer, Scale-free, programmable design of morphable chain loops of kilobots and colloidal motors. *Proc. Natl. Acad. Sci. U.S.A.* **117**, 8700–8710 (2020).
40. M. Spellings, M. Engel, D. Klotsa, S. Sabrina, A. M. Drews, N. H. P. Nguyen, K. J. M. Bishop, S. C. Glotzer, Shape control and compartmentalization in active colloidal cells. *Proc. Natl. Acad. Sci. U.S.A.* **112**, E4642–E4650 (2015).
41. W. Mickel, S. C. Kapfer, G. E. Schröder-Turk, K. Mecke, Shortcomings of the bond orientational order parameters for the analysis of disordered particulate matter. *J. Chem. Phys.* **138**, 044501 (2013).
42. F. Kümme, B. ten Hagen, R. Wittkowski, I. Buttinoni, R. Eichhorn, G. Volpe, H. Löwen, C. Bechinger, Circular motion of asymmetric self-propelling particles. *Phys. Rev. Lett.* **110**, 198302 (2013).
43. A. Pototsky, U. Thiele, H. Stark, Mode instabilities and dynamic patterns in a colony of self-propelled surfactant particles covering a thin liquid layer. *Eur. Phys. J. E* **39**, 51 (2016).
44. P. Eshuis, K. van der Weele, D. Lohse, D. van der Meer, Experimental realization of a rotational ratchet in a granular gas. *Phys. Rev. Lett.* **104**, 248001 (2010).
45. J. Schwarz-Linek, C. Valeriani, A. Cacciuto, M. E. Cates, D. Marenduzzo, A. N. Morozov, W. C. K. Poon, Phase separation and rotor self-assembly in active particle suspensions. *Proc. Natl. Acad. Sci. U.S.A.* **109**, 4052–4057 (2012).
46. C. Maggi, F. Saglimbeni, M. Dipalo, F. De Angelis, R. Di Leonardo, Micromotors with asymmetric shape that efficiently convert light into work by thermocapillary effects. *Nat. Commun.* **6**, 7855 (2015).
47. S. Sacanna, W. T. M. Irvine, P. M. Chaikin, D. J. Pine, Lock and key colloids. *Nature* **464**, 575–578 (2010).
48. S. Ni, J. Leemann, I. Buttinoni, L. Isa, H. Wolf, Programmable colloidal molecules from sequential capillarity-assisted particle assembly. *Sci. Adv.* **2**, e1501779 (2016).
49. B. Yigit, Y. Alapan, M. Sitti, Cohesive self-organization of mobile microrobotic swarms. *Soft Matter* **16**, 1996–2004 (2020).

Acknowledgments: We thank E. Altshuler for inspiring discussions. **Funding:** This work was supported by Deutsche Forschungsgemeinschaft (grant nos. SCHO 1700/1-1, LO 418/23-1) to C.S. and H.L., respectively. M.E. acknowledges the Cluster of Excellence Engineering of Advanced Materials Grant EXC 315/2. TP and ME thank the Interdisciplinary Center for Nanostructured Films (IZNF), the Central Institute for Scientific Computing (ZISC), and the Interdisciplinary Center for Functional Particle Systems (FPS) at Friedrich-Alexander University Erlangen-Nürnberg. Computational resources and support provided by the Erlangen Regional Computing Center (RRZE) are gratefully acknowledged. **Author contributions:** C.S. and A.L. performed and evaluated the experiments. M.E. performed and evaluated the simulations. All authors discussed the results and wrote the manuscript. **Competing interests:** The authors declare that they have no competing interests. **Data and materials availability:** All data needed to evaluate the conclusions in the paper are present in the paper and/or the Supplementary Materials. Additional data related to this paper may be requested from the corresponding author.

Submitted 26 November 2020

Accepted 25 February 2021

Published 14 April 2021

10.1126/sciadv.abf8998

Citation: C. Scholz, A. Ldov, T. Pöschel, M. Engel, H. Löwen, Surfactants and rotelles in active chiral fluids. *Sci. Adv.* **7**, eabf8998 (2021).

Surfactants and rotelles in active chiral fluids

Christian Scholz, Anton Ldov, Thorsten Pöschel, Michael Engel and Hartmut Löwen

Sci Adv 7 (16), eabf8998.
DOI: 10.1126/sciadv.abf8998

ARTICLE TOOLS

<http://advances.sciencemag.org/content/7/16/eabf8998>

SUPPLEMENTARY MATERIALS

<http://advances.sciencemag.org/content/suppl/2021/04/12/7.16.eabf8998.DC1>

REFERENCES

This article cites 48 articles, 8 of which you can access for free
<http://advances.sciencemag.org/content/7/16/eabf8998#BIBL>

PERMISSIONS

<http://www.sciencemag.org/help/reprints-and-permissions>

Use of this article is subject to the [Terms of Service](#)

Science Advances (ISSN 2375-2548) is published by the American Association for the Advancement of Science, 1200 New York Avenue NW, Washington, DC 20005. The title *Science Advances* is a registered trademark of AAAS.

Copyright © 2021 The Authors, some rights reserved; exclusive licensee American Association for the Advancement of Science. No claim to original U.S. Government Works. Distributed under a Creative Commons Attribution NonCommercial License 4.0 (CC BY-NC).